VII Bis-ThCBM as an acceptor in P3HT based bulk heterojunction solar cells

This chapter details the optimisation of bulk heterojunction solar cells containing poly(3-hexyl thiophene) and bis-[6,6]-thienylC_{61} butyric acid methyl ester. It has been found that optimised bis-ThCBM based devices obtained an efficiency of 4.6% compared to 3.6% for optimised PCBM based devices. The efficiency improvement results mainly from a superior open circuit voltage of 0.69V compared to 0.59V. In addition, external quantum efficiency measurements and critical field modelling suggest that bis-ThCBM provides improved charge extraction towards the high energy end of the visible spectrum.

VII.I Introduction

A brief examination of the power conversion efficiency (PCE) equation for solar cells shows that PV efficiency can be improved by either increasing the short circuit current (I_{SC}), open circuit voltage (V_{OC}), or the fill factor (FF), for a given incident light power density, (P_S).

$$\mathrm{PCE} = \frac{\mathrm{I_{SC}\,V_{OC}\,FF}}{\mathrm{P_S}} \qquad (1)$$

As was discussed in Chapter 3, the V_{OC} in polymer/fullerene composite solar cells is limited by the difference between the HOMO of the polymer species ($HOMO_{donor}$) and the LUMO of the fullerene species ($LUMO_{acceptor}$)[1,2,3]. In Chapter 6, a number of fullerene derivatives were investigated in order to determine their LUMO levels relative to PCBM and bis-ThCBM was found to be the most promising for incorporation into photovoltaic devices.

To this end the modified fullerene bis-[6,6]-thienyl-C_{61}-butyric acid methyl ester (bis-ThCBM) has been incorporated into P3HT based bulk-heterojunction photovoltaic devices with the results presented herein. Bis-ThCBM is the bisadduct of thienyl-C_{61}-butyric acid methyl ester, as shown in Figure 1. ThCBM is similar to the more familiar PCBM but is differentiated by the incorporation of a thienyl group in place of the phenol. This switch was motivated by the hypothesis that the thienyl group may provide improved conformity with polythiophene polymers, specifically P3HT[4]. BisThCBM is obtained as a byproduct of ThCBM synthesis and separated using liquid chromatography. The bis-ThCBM used in these experiments was purchased from Solenne BV and contains a mixture of 17 isomers[5] with the second addend located at various positions on the fullerene cage.

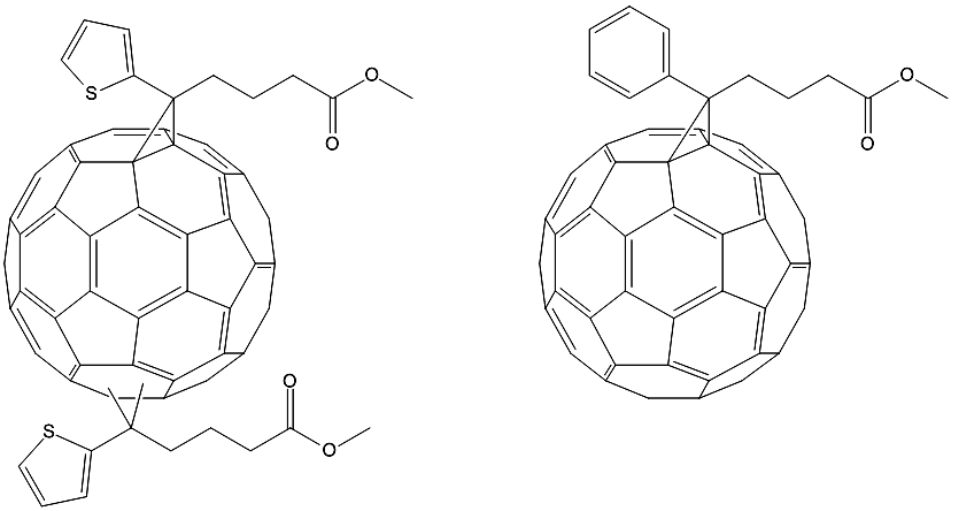

Figure 1. Chemical structures of bis-ThCBM (left) and PCBM (right).

VII.II Electronic Properties of bis-ThCBM

In chapter 6, the electrochemistry of bis-ThCBM was investigated by cyclic voltammetry and revealed a LUMO level approximately 100 meV above that of PCBM. In addition, it was deemed prudent to investigate the molecules electron mobility.

VII.II.I Electron Mobility of bis-ThCBM

The electron mobility of bis-ThCBM is a key parameter because it would directly influence the drift velocity of dissociated electrons in a photovoltaic device. High mobilities are required in order to limit recombination and obtain good fill factors and high efficiencies. Electron mobility can be determined via a number of experimental techniques including field effect transistors,[6] time-of-flight measurements[7] and by the analysis of space-charge limited current (SPLC) characteristics in the dark[4,8,9]. Of the methods available, SCLC analysis was chosen

for this work as it provides the most accurate imitation of photovoltaic device conditions and fits most neatly with the equipment and expertise in our laboratory. A full explanation of the theory underpinning the determination of charge carrier mobilities from SCLC data along with the methods used to produce the electron only devices required for this work are presented in Chapter 3.

Figure 2 presents the experimental dark current densities of a bis-THCBM device and a PCBM device and the fitted SCLC models. The data shows that the devices exhibits classic SCLC behaviour above 0.2V. Using SCLC theory as outlined in Chapter 3 a zero field electron mobility of 0.5 (±0.3) x 10^{-7} $m^2V^{-1}s^{-1}$ was obtained for bis-ThCBM which is similar to the reported electron mobility of bis-PCBM (0.7 x 10^{-7} $m^2V^{-1}s^{-1}$)[8]. For PCBM a zero field mobility of 1.7 x (± 0.4) 10^{-7} $m^2V^{-1}s^{-1}$ was calculated, which matches well with the literature value of 2 x 10^{-7} $m^2V^{-1}s^{-1}$.[10] and is similar to the electron mobility reported for ThCBM of 1.8(±0.8) x 10^{-7} $m^2V^{-1}s^{-1}$. [4]

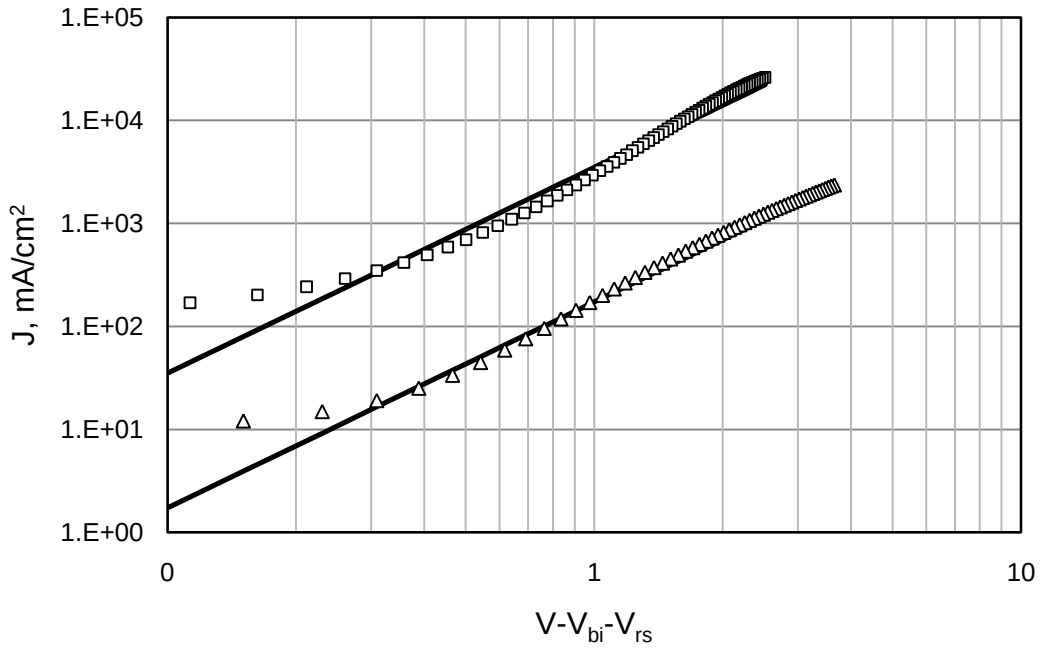

Figure 2. J-V curve of an ITO/PEDOT:PSS:bbis-PCBM/LiF/Al (squares) and a ITO/PEDOT:PSS:bis-ThCBM/LiF/Al device (triangles). Hollow squares/triangles show experimental results while the solid line represents model SCLC behaviour. R_s = 20Ω, V_{bi} = 1.4V. PCBM layer thickness = 110nm. Bis-ThCBM layer thickness = 120nm.

The electron mobility of the bis-derivatives is generally lower because the second addend inhibits close packing of the fullerene and limits the number of possible intermolecular configurations with π orbital overlap. This effect is exacerbated by the large number of isomers present within the sample with the result being a reduction in the electron mobility. In spite of this, it is likely that the electron mobility of bis-ThCBM is still high enough to anticipate a charge balanced photovoltaic device when combined with P3HT, as the hole mobility in P3HT:ThCBM films has been reported to be only 0.2×10^{-7} $m^2V^{-1}s^{-1}$.[11]

VII.III Optimisation of P3HT:bis-ThCBM solar cells

Following the determination of its electron mobility, bis-ThCBM was incorporated into bulk heterojunction photovoltaic devices. A wide range of process variables can be manipulated during the fabrication of solution processed photovoltaic devices. These include the spin casting solvent, the polymer:fullerene ratio, the absolute solute concentrations, the solution age, the spin casting speed, the active layer drying time, the electrode composition and deposition rate and the annealing temperature and duration.

In this work, P3HT:bis-ThCBM devices were spin cast from chlorobenzene (CB) and ortho-dichlorobenzene (DCB) solutions. The P3HT concentration was kept constant at 10mg/mL P3HT while P3HT:bis-ThCBM ratios were varied from 1:0.5 to 1:1.3. DCB is slightly more viscous than CB and has a higher boiling point (180°C compared to 132°C). This difference leads to a longer drying time for DCB based films and therefore requires a slightly altered fabrication method. CB based devices dry during the spin casting process (< 30sec) and perform best following a post production anneal as related in Chapter 3. DCB based devices can take hours to dry after the spin casting process. This allows for the re-orientation of polymer and fullerene components in the active layer which reduces the need for a post production heat treatment. All devices were spin cast for 30 seconds at 700 rpm, after which CB based devices were dry enough to be placed in the evaporator. DCB based devices on the other hand were left to dry overnight to allow excess solvent to evaporate.

The following figures 3 - 8, relate the device parameters of fabricated solar cells. Each data point represents three solar cells from a single substrate, with the error bars representing one standard deviation from the mean. In some cases, where the cells from a single substrate showed large variations in their device parameters, values for each pixel have been plotted and possible reasons for the variation are discussed in the text. Blue data points relate to the left axis and red data points relate to the right axis.

All white light efficiency results presented herein were checked by calculating the expected white light short circuit current from the EQE results. Comparisons of the measured and calculated J_{SC}s for the devices fabricated with an interfacial LiF layer are presented in the Appendix. One the whole, the values calculated from the EQE results match within 10% of the actual J-V measurements. The observed variations are due to the difference between the spectrum of solar simulator light source and the AM1.5 spectrum and because of the lack of a white light bias in the EQE set up.

VII.III.I P3HT:bis-ThCBM Devices spin cast from Chlorobenzene

Figure 3 presents the J-V results for a series of devices spin cast from chlorobenzene (CB) with a 10 minute post fabrication heat treatment at 150°C. It can be seen that the J_{SC} peaks at 8.4 mA/cm^2 for a P3HT:bis-ThCBM weight ratio of 1:0.9. Although this is higher than the 1:0.8 weight ratio reported to be optimal for P3HT:PCBM devices,[12] it is approximately equal as a molar ratio. From left to right across the graph there is a weak positive trend for increasing J_{SC} due to the steadily increasing device thickness and related light absorption. The devices gradually increase in

thickness from 85 nm to 112 nm because the solutions from which they are spin cast increase in viscosity as the fullerene concentration increases. Thickness changes could have been compensated for by altering the spin casting speed, or polymer concentration but these options would have led to variations in drying time which would have also affected device parameters.

Although increased thickness results in improved absorption, it also leads to (for a given P3HT:fullerene ratio) an increased series resistance and increased charge carrier transit times. The former reduces the fill factor, while the later increases recombination. In addition, at low bis-THCBM ratios, the P3HT:bis-ThCBM interfacial area is not optimised. This limits the potential for exciton separation and also means that the bis-ThCBM percolation network necessary for effective electron transport is not fully developed. As the bis-PCBM ratio increases, both the interfacial area and the bis-ThCBM percolation network improve. As a result, J_{SC} increases.

Beyond a certain point, in this case a P3HT:bis-ThCBM ratio of 1:0.9, it is likely that the converse begins to happen. Extrapolating from the P3HT:PCBM system, as Bis-ThCBM becomes the dominant volumetric phase, the interfacial area declines and the P3HT percolation network is impeded. The observed drop in J_{SC} at high bis-ThCBM ratios can be attributed to excessive coarsening of the P3HT:bis-ThBCM morphology as a result of the annealing process. As shown in Chapter 4, annealing causes phase segregation in polymer:fullerene solar cells, which on a small scale can be beneficial for device performance. However, for long annealing times, or high fullerene concentrations, the coarsening can become excessive[13,14]. AFM is one

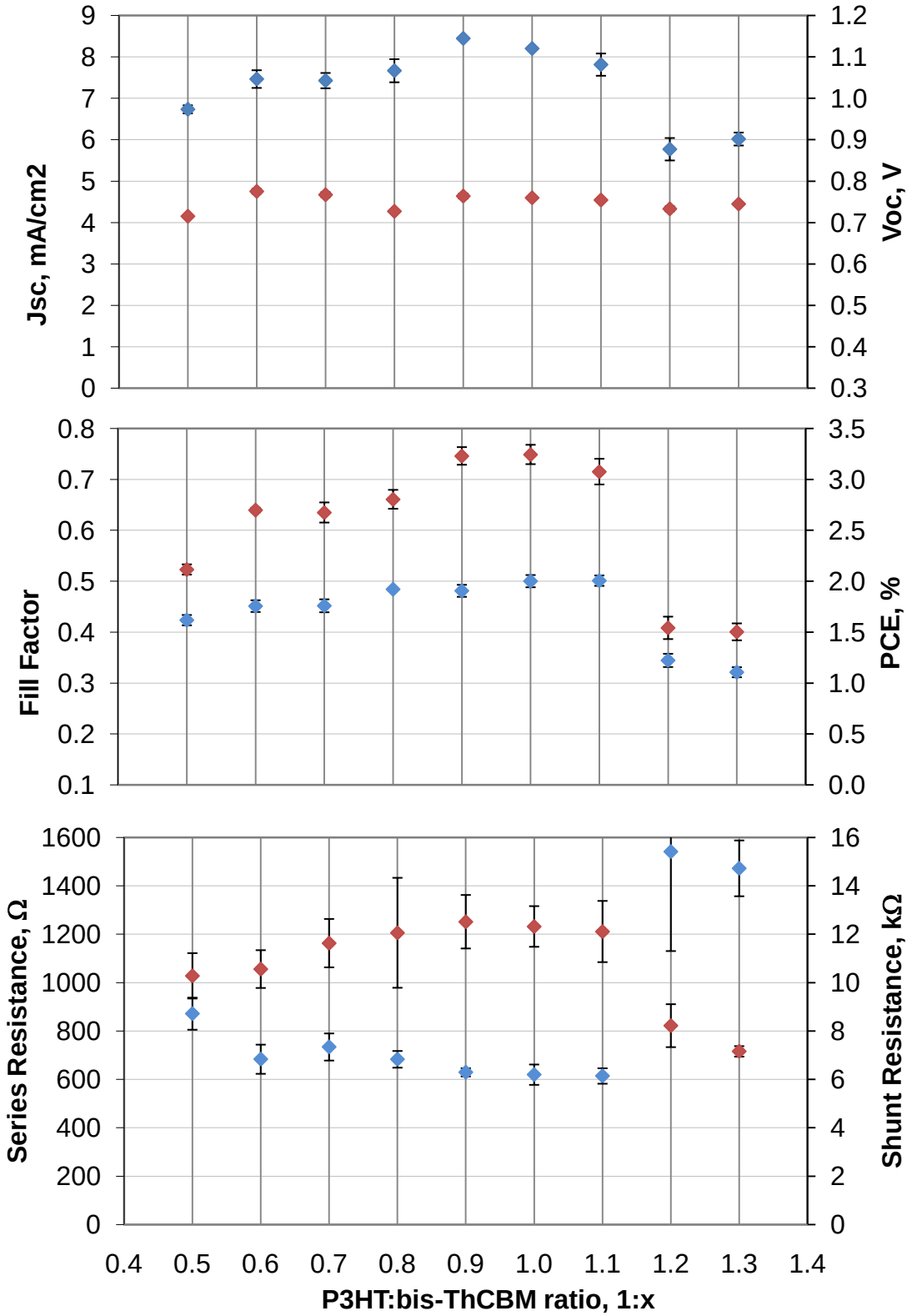

Figure 3. P3HT:bis-ThCBM, chlorobenzene as solvent, 10 min heat treatment at 150°C. Blue diamonds = left axis. Red diamonds = right axis.

method that is useful for probing the morphology of polymer thin films. Due to the very thin nature of the polymer:fullerene film, changes in surface roughness can be taken as a proxy for morphological changes in the film 'bulk'. Figure 4 presents root mean squared (RMS) roughness values, extracted from atomic force micrographs, for the devices presented in Figure 3. Interestingly, the RMS roughness values are stable below a polymer:fullerene ratio of 1:0.8. However, above this, RMS roughness increases sharply, indicating increased morphological coarsening. This coincides with the decline in J_{SC} observed in Figure 3 beyond a polymer:fullerene ratio of 1:0.9.

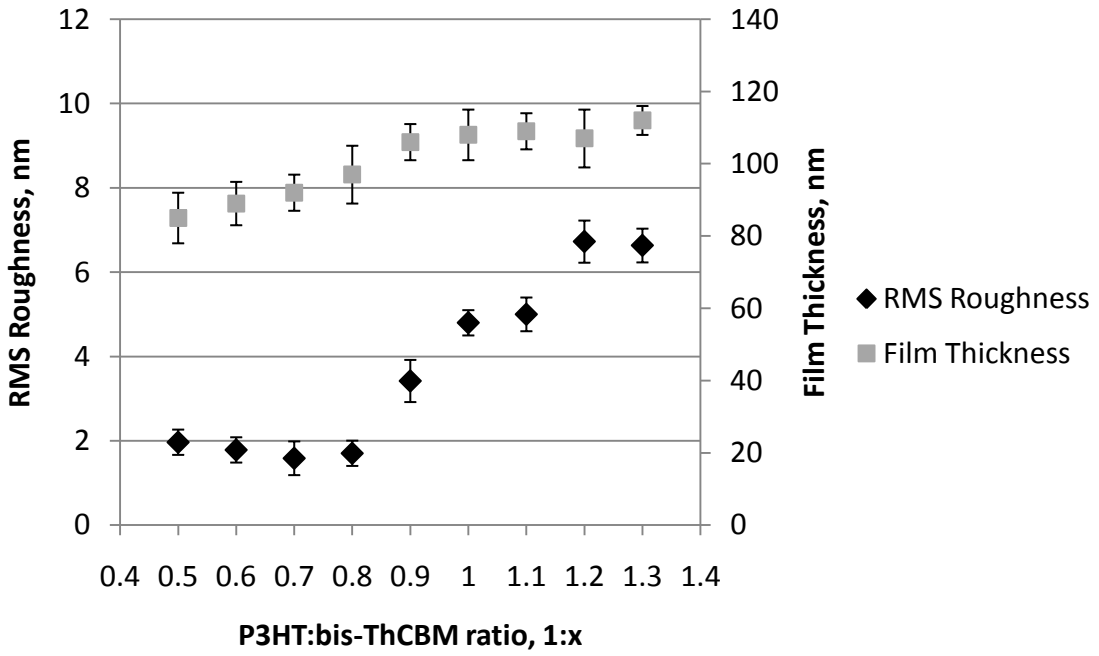

Figure 4 RMS Roughness and Thickness Measurements of Devices from Figure3. P3HT:bis-ThCBM, chlorobenzene as solvent, 10 min heat treatment at 150°C.

It can also be seen in Figure 3 that the V_{OC} is fairly steady over the range of bis-ThCBM ratios, reaching a maximum of 0.78V at a ratio of 1:0.6. This is a 25% increase

over typical V_{OC}s found in P3HT:PCBM solar cells (0.62V) and is one of the highest V_{OC}s reported for P3HT:fullerene based solar cells.

The fill factor is highly dependent on morphology and as such, it follows a similar trend to the J_{SC}. Initially, increases in bis-ThCBM content improve the bicontinuous morphology, which reduces the series resistance and improves the FF. At high bis-ThCBM loadings, it is likely that the increased phase coarsening retards the P3TH percolation network and this, in conjunction with the increasing film thickness, leads to a significant increase in the series resistance R_S. The shunt resistance, R_{SH} shows an almost opposite trend. It exhibits a positive correlation with bis-THCBM concentration as the improving morphology reduces charge carrier recombination. In addition, thicker devices are less susceptible to micro shorts which provide an additional positive trend in R_{SH} from left to right. The shunt resistance plateaus as the morphology is optimised and then drops in the bis-THCBM rich devices as coarsening becomes excessive and recombination increases.

The power conversion efficiency (PCE) represents the net effect of all these factors and is dominated by the reinforcing trends of the J_{SC} and FF. A maximum efficiency of 3.2% is achieved at a P3HT:bis-THCBM ratio of 1:0.9/1.0. As mentioned previously, this correlates well on a molar basis with the optimal ratio for P3HT:PCBM devices of 1:0.8.

VII.III.II P3HT:bis-ThCBM Devices spin cast from ortho-dichlorobenzene (DCB)

Having obtained these promising results in chlorobenzene based devices it was then hoped that further improvements could be achieved using DCB.[7]

Figure 5 presents J-V parameters for devices spin cast from DCB. Devices were subjected to a 5 minute annealing treatment at 150°C after the thermal deposition of an Al cathode. Considerable differences are evident in the trends for all device parameters compared to the CB based devices. Firstly, J_{SC} values are broadly higher. This can be explained in part by the increased film thickness in the DCB based devices. Dektak measurements show that the films cast from CB range from 90 to 110nm in thickness depending on the fullerene loading, while the films cast from DCB are 180 – 260nm thick. The increased thickness is a result of the more viscous nature of the DCB solutions and the practice of removing the devices from the spin coater while still wet instead of spin coating to dry. The increased thickness leads to increased absorption and charge generation.

In addition, as can be seen in Figure 6, devices cast from DCB exhibit a broader EQE response with EQE turn-on occurring more steeply. The more pronounced shoulder between 600-650nm has been previously correlated with improved π-π stacking in P3HT[15,16] which suggests improved P3HT crystallinity within the DCB cast devices. The improved EQE at shorter wavelengths is likely due to a combination of improved charge carrier mobility and absorption.

The J_{SC} values also peak at a higher bis-ThCBM loading (1:1.3) for devices spin cast from DCB. This is also indicative of improved crystallinity within the P3HT rich phase, which should be more effective at maintaining hole transport at high bis-ThCBM volume fractions.

Further support for improved packing in the DCB based devices can be seen in the fill factors, which are broadly higher than for the CB based devices, despite the increased film thickness. This implies an improvement in charge transport, allowing for efficient charge extraction from a significantly thicker film, and is supported by the comparatively low R_S values.

.

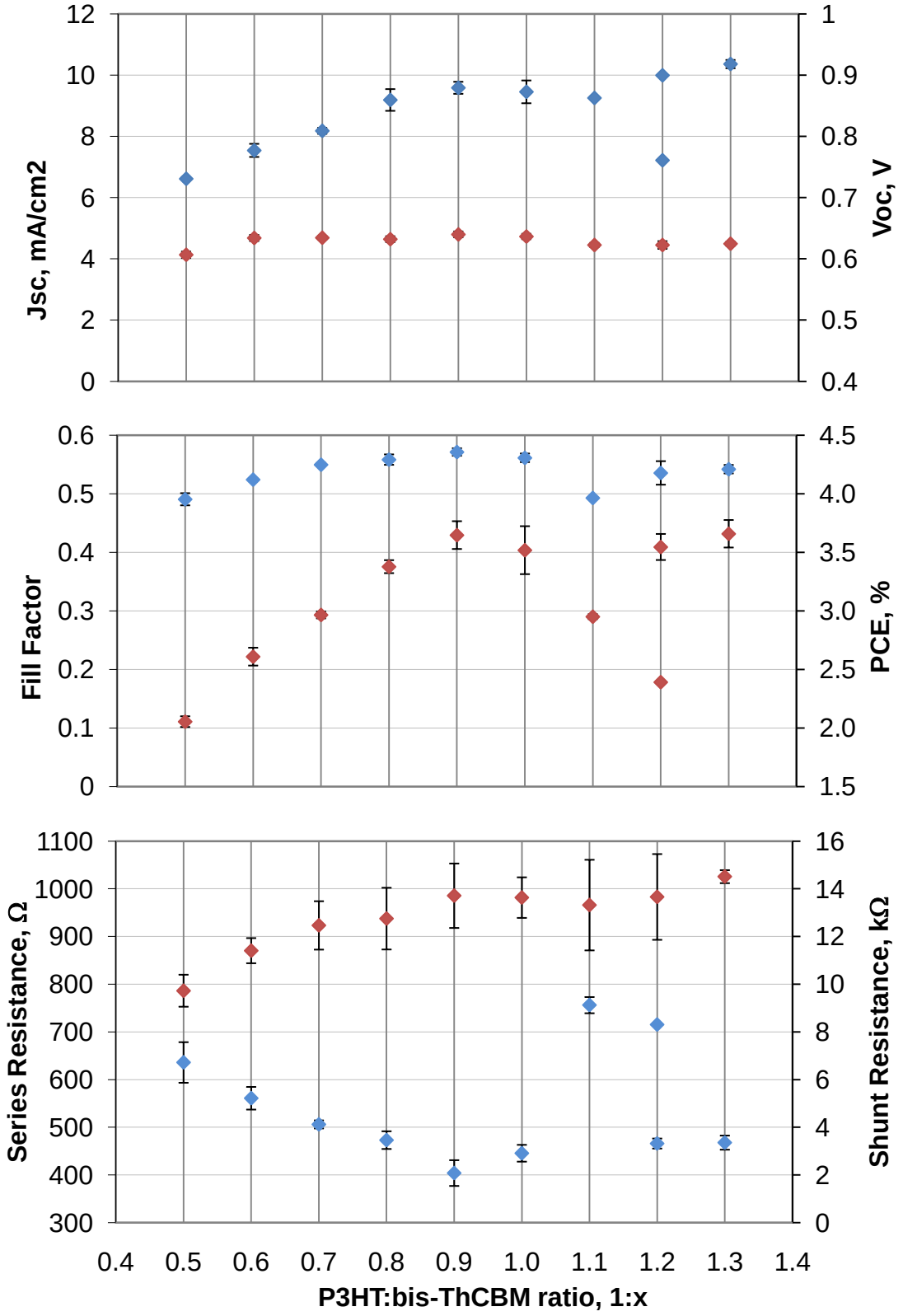

Figure 5. P3HT:bis-ThCBM, dichlorobenzene as solvent, 5min HT at 110°C after Al dep. Blue diamonds = left axis. Red diamonds = right axis.

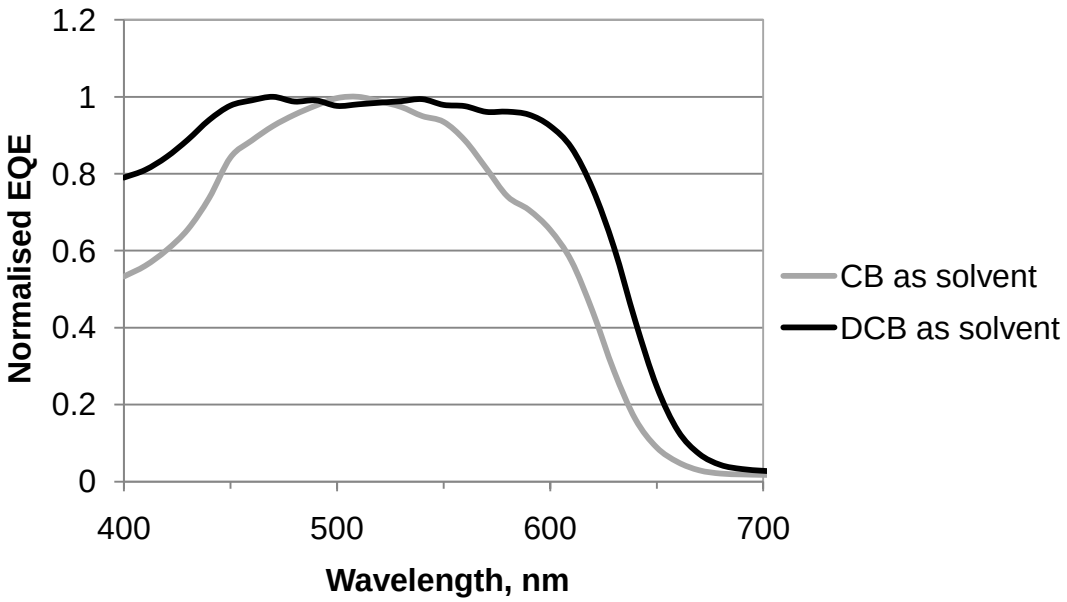

Figure 6. External Quantum Efficiency (EQE) results comparing P3HT:bis-ThCBM devices spin cast from Chlorobenzene and Dichlorobenzene.

In the top graph of Figure 5, one can see there is significant variation in the J_{SC} at high bis-ThCBM loadings, within a single device. As can be seen most clearly at a ratio of 1:1.1 and 1:1.2, variations in the short circuit current and fill factor is observed. Optical microscopy of the device surface showed that at high concentration, relatively large fullerene agglomerates begin to appear within the polymer film. These agglomerates act to shadow the photoactive film below them causing a reduction in short circuit current. In addition, the agglomerates reduce the polymer:fullerene interfacial area within the film and disrupt the bicontinuous morphology, hampering exciton dissociation and charge transport.

By chance, most devices were free of fullerene agglomerates and showed superior performance, (represented by the higher data points for 1:1.1 and 1:1.2 ratios in

Figure 5). Interestingly, the highest J_{SC}, and device efficiency is obtained for the highest bis-THCBM loading investigated.

Atomic force micrographs reveal that overall, the DCB based devices exhibit significantly higher RMS roughness values than the CB based devices and a weaker correlation between RMS roughness and the fullerene concentration. This suggests that morphological change is less pronounced in DCB based devices. However, considering the increased device thicknesses, it is more problematic to assume a correlation between surface roughness and bulk morphology.

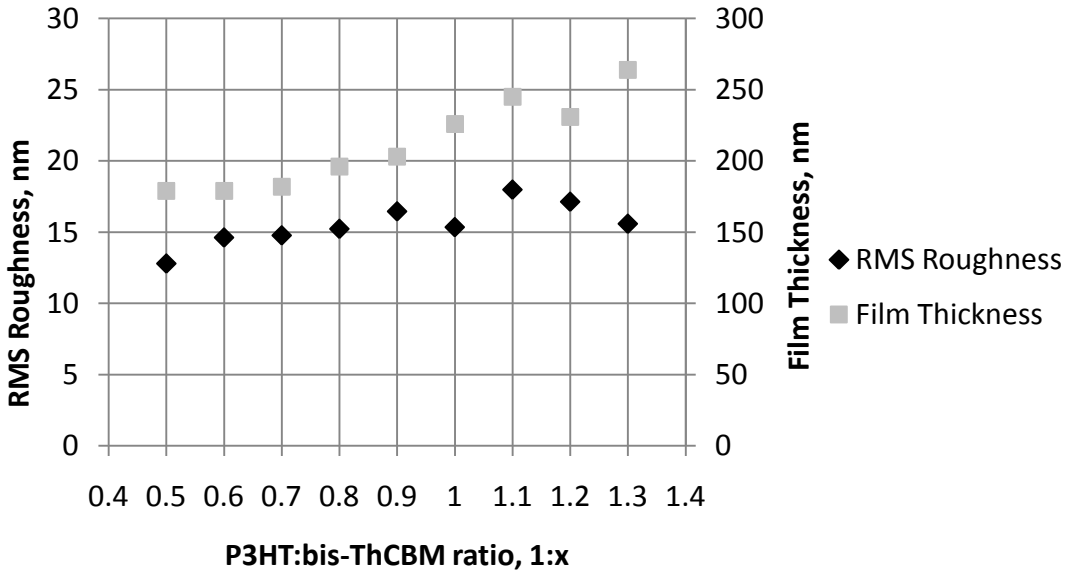

Figure 7. RMS Roughness and Dektak thickness measurements of devices from Figure 5. P3HT:bis-ThCBM, 1,2-dichlorobenzene as solvent, 5 min heat treatment at 110°C after Al deposition.

Another interesting point to note from Figure 5 is that the use of DCB appears to reduce the open circuit voltage by over 0.1V to approximately 0.65V. Many variations of annealing time and temperature were investigated to increase the V_{OC}

of the devices cast from DCB but none proved successful. Further investigation of the open circuit voltage is presented in the section below.

VII.III.III Origin of the V_{OC} variation in P3HT:bis-ThCBM solar cells

There are four main factors that affect the V_{OC} in polymer fullerene solar cells. As discussed in previous chapters, the V_{OC} is strongly linked to the difference between the polymer HOMO and the fullerene LUMO. In addition, the V_{OC} can also be increased by incorporating low work function cathode materials, [3] although this effect is mitigated by Fermi level pinning of the cathode to the fullerene LUMO.[17,18] Thirdly, a number of studies have shown that V_{OC} decreases with increasing fullerene concentration.[19,20,21] It has been stated that this effect is due to the influence of fullerene coverage at the semiconductor/cathode interface[20] but it is not immediately clear why this might be the case. It is possible that increased fullerene concentrations at the interface lead to stronger pinning of the cathode Fermi level to the fullerene LUMO, resulting in a depression in the device's built in field and therefore V_{OC}. Fourthly, the spin casting solvent has also been shown to affect the V_{OC}. Recent XPS[22] and variable-angle spectroscopic ellipsometry (VASE) results[13] regarding the vertical segregation of P3HT:PCBM films have indicated that slow grown films, such as those spin cast from DCB, exhibit higher fullerene concentration at the cathode interface than fast grown, annealed films. In addition, a study by Yang Yang et al. showed that devices spin cast from aromatic solvents yielded lower V_{OC}s than devices cast from non-aromatic solvents.[20] The authors proposed that aromatic solvents were more inclined to solvate the conjugated groups of the polymer chains, allowing for improved interfaces between the conjugated groups of

the polymer and fullerene and yielding a lowered V_{OC}. It is possible that a more polar solvent would reduce the interfacial barrier to exciton dissociation across the polymer/fullerene interface, effectively reducing the $LUMO_{donor}$ – $HOMO_{acceptor}$ offset and therefore the V_{OC}. This would seem to match with the EQE comparison of CB and DCB based devices in Figure 6, whereby the DCB based devices exhibit EQE turn-on at a lower energy (longer wavelength), suggesting a lower threshold is required in order to excite and dissociate an exciton.

In addition, the improved P3HT packing that the use of DCB facilitates, likely leads to an increased average conjugation length along the polymer backbone.[23] This would act to raise the polymer HOMO, reducing the polymer bandgap, and therefore the $LUMO_{donor}$ – $HOMO_{acceptor}$ offsert and the V_{OC}. This also fits with the lower energy turn-on observed in the EQE spectra in Figure 6. However, it cannot be the full story as the shift in EQE turn on of 13nm correlates to a 0.04 eV reduction in the polymer bandgap. Even assuming that this reduction is caused solely by an increase in the HOMO, with no reduction in the LUMO, it still only accounts for less than 50% of the observed decrease in V_{OC} (≈0.13V).

All these factors begin to suggest why there are notable differences in V_{OC} between devices cast from different solvents and with different heat treatment regimes. As the V_{OC} trends negatively with increasing concentration at the semiconductor/Al interface, and slow-dried films have been shown to exhibit higher fullerene concentrations at the interface,[13,22] one can conclude that films cast from DCB should exhibit a lower V_{OC}. In addition, as DCB is more miscible with the solutes than

CB, the effects observed by Yang Yang may also come into play, with an improved polymer/fullerene interface leading to a reduced V_{OC} in DCB cast device and an increase in the polymer conjugation length leading to a raise polymer HOMO. The solvent and processing conditions appear to have a more acute effect on the V_{OC} of bis-ThCBM based devices than on PCBM based devices, as can be seen in Table 1. Bis-ThCBM devices exhibit an overall V_{OC} variation of 0.26V compared to 0.08V for the PCBM devices.

Device Type	**V_{OC} P3HT:bis-ThCBM, V**	**V_{OC} P3HT:PCBM, V**
CB	0.76 ± 0.03	0.64 ± 0.02
DCB, HT before Al	0.50 ± 0.01	0.56 ± 0.01
DCB, HT after Al	0.63 ± 0.01	0.59 ± 0.01
DCB LiF	0.70 ± 0.01	0.60 ± 0.01

Table 1. V_{OC} values for devices spin cast from different solvents, with and without LiF layers. CB devices were heat treated at 150°C for 10 minutes after Al evap. DCB devices were heat treated at 110°C for 5 minutes. DCB devices with LiF were not heat treated.

Although annealing has primarily been investigated as it relates to J_{SC} and the series resistance, it is clear from Table 1 that it can also have an effect on V_{OC}. Several reports have been published that deal qualitatively with the effect of annealing on the polymer/cathode interface, with several suggesting an improvement in adhesion strength and contact area.[12,24,25,26] Most recently, Kim et al. have used synchrotron x-rays to develop models of the Al distribution at the organic/Al interface[27] and showed that annealing leads to the diffusion of Al into the polymer film, disrupting the preferential alignment of P3HT crystallites and reducing the contact resistance and injection barrier at the interface. It is likely that such a reduction in the injection

barrier is responsible for the difference in V_{OC} observed in Table 1 between devices heat treated before and after Al deposition. In addition, synchrotron x-ray[22] work and VASE[13] experiments both suggest that annealing appears to reduce the fullerene concentration at the interface, which would further aid the V_{OC}.

VII.III.IV The incorporation of a LiF interfacial cathode layer

The one technique that was found to successfully restore the V_{OC} in devices spin cast from DCB was the introduction of a very thin (1 nm) lithium fluoride (LiF) layer between the polymer/fullerene layer and the Al. At this thickness, LiF does not form a continuous layer, but instead consists of small clusters scattered across the polymer surface. The benefits of a thin interfacial LiF layer were first observed in organic LEDs (OLEDS) where it was shown to enhance charge injection and quantum efficiency and reduce the operating voltage due to its ability to reduce the electron injection barrier at the cathode. [28,29,30,31,32]

A similar effect occurs in photovoltaics. When deposited between the polymer and metal cathode layers, LiF forms a dipole moment across the interface with Li^+ oriented towards the polymer and the F^- pointing towards the metal.[33] The strong dipole moment creates a vacuum level offset which effectively lowers the metal cathode work function,[33] thereby reducing the voltage loss at the cathode interface. In addition, LiF can perform a protective function, by preventing the formation of Al-organic complexes at the interface that create an insulting layer.[34]

As a result, LiF has been shown to increase the fill factor and V_{OC} in polymer:fullerene based photovoltaic devices and both effects are seen here in Figure 8, with V_{OC} increasing to approximately 0.7V and the fill factor improving slightly to 0.59. As a result, the devices incorporating the interfacial LiF layer delivered the highest efficiencies reaching 4.6% at a P3HT:bis-THCBM ratio of 1:1.3. Similar trends were observed in PCBM based devices (Figure 9) fabricated using an identical procedure with a maximum efficiency of 3.6%. The major difference between the two sets of devices is the V_{OC}, which accounts for 75% of the difference in device efficiency. The bis-THCBM device was slightly thicker, at 285nm, compared to the PCBM device at 250nm which helps explain the slightly higher J_{SC}. However, despite the increased thickness, the bis-THCBM device exhibits a slightly higher fill factor (0.60 vs. 0.57) and lower series resistance. The improved fill factor is likely the result of improved charge carrier mobility, but the electron mobility of bis-ThCBM has already been shown to be slightly lower than that of PCBM (Figure 2). To determine whether improved hole mobility plays a role, SCLC hole mobility experiments were carried out and are discussed in section VI.III.IV below.

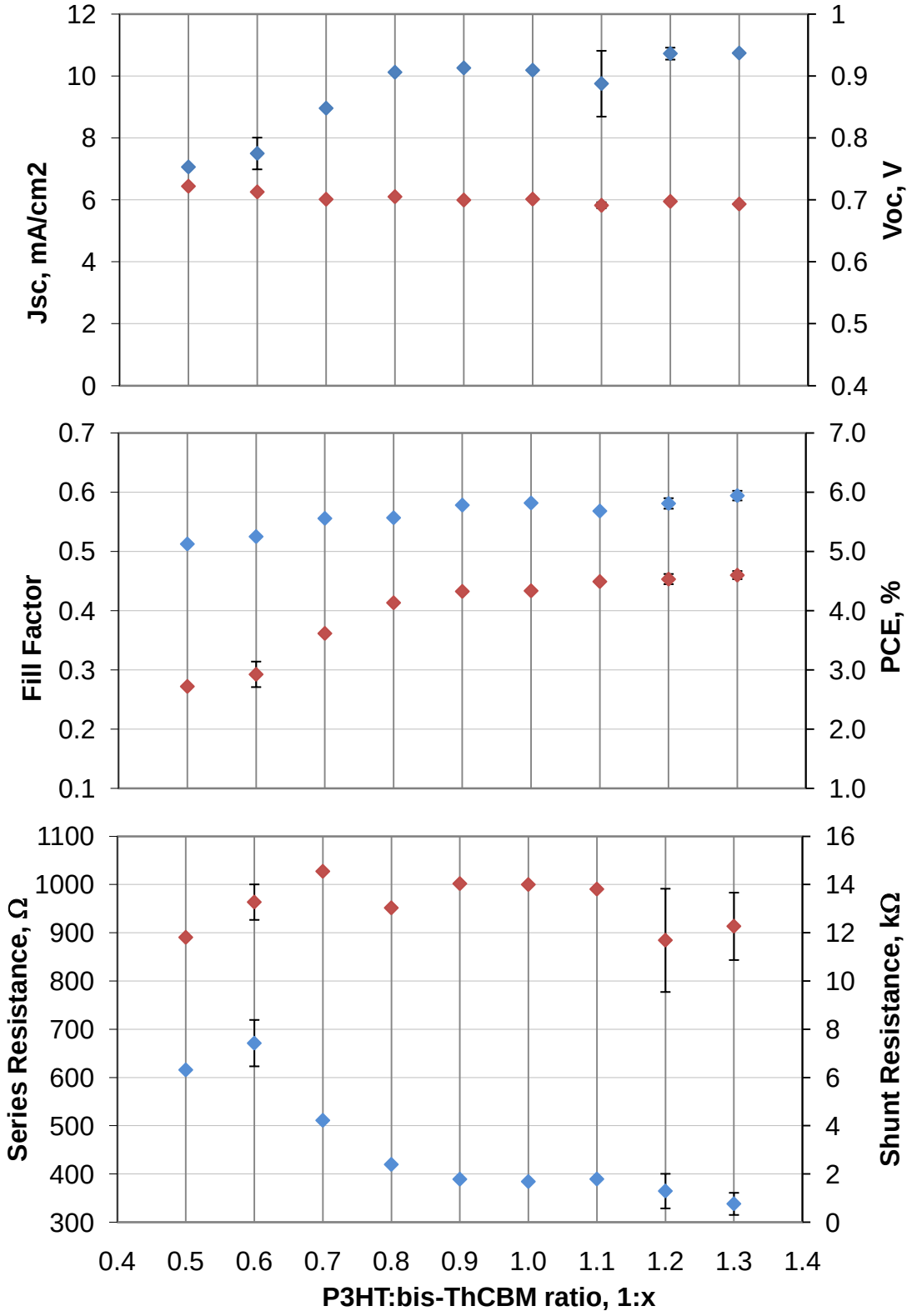

Figure 8. P3HT:bis-ThCBM, dichlorobenzene as solvent, LiF and Al, no HT. Blue diamonds = left axis. Red diamonds = right axis.

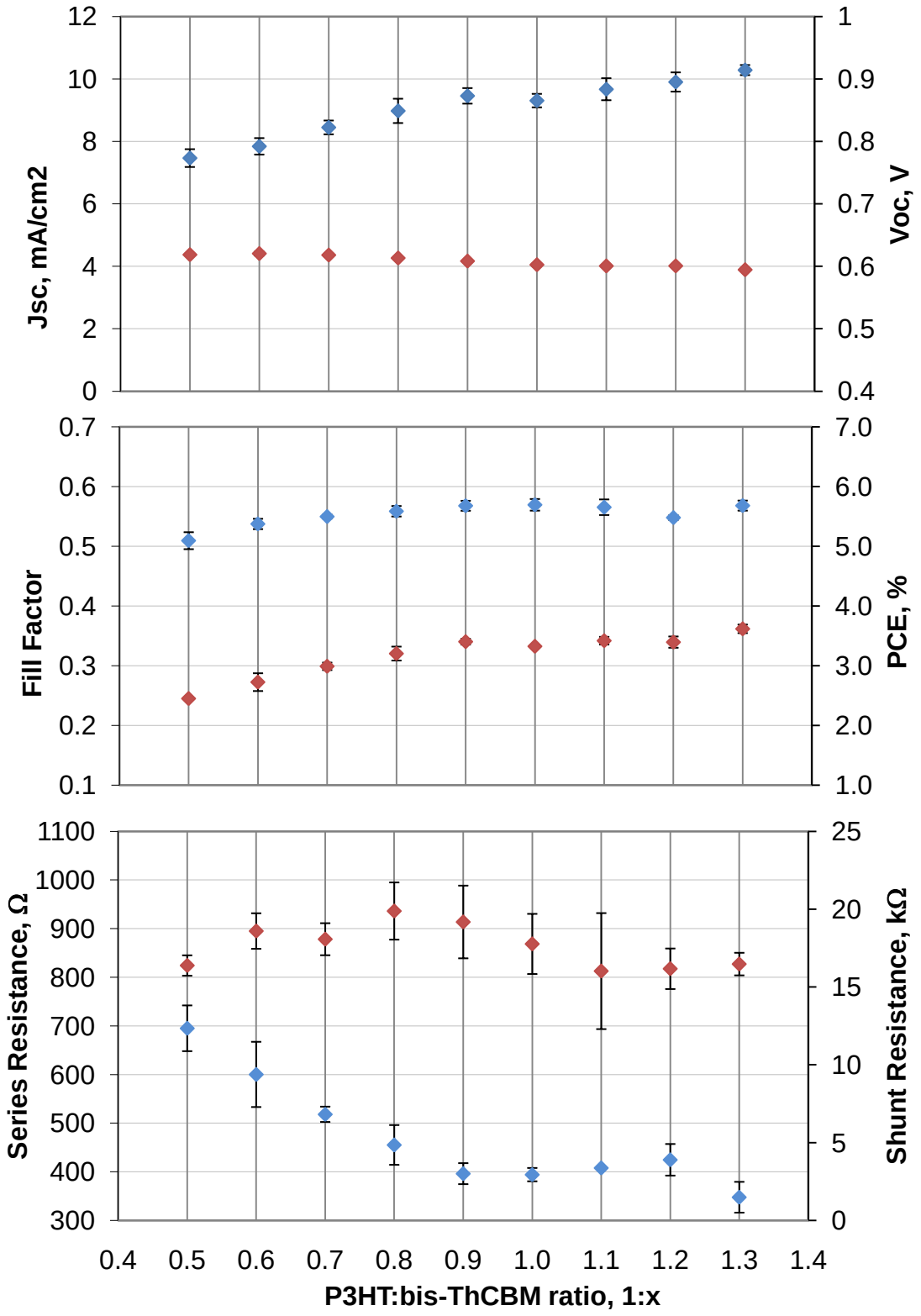

Figure 9. P3HT:PCBM, dichlorobenzene as solvent, LiF and Al, no HT. Blue diamonds = left axis. Red diamonds = right axis.

VII.IV Hole Mobility of P3HT:fullerene solar cells determined by SCLC Measurements

To investigate the impact of bis-ThCBM on the hole mobility in polymer:fullerene devices, SCLC hole mobility measurements were conducted, as similarly used for extracting the electron mobility from bis-ThCBM thin films. However, instead of using a LiF/Al electrode to prevent hole injection from the anode, a Palladium cathode is used. With a work function of 5.2eV, Palladium prevents electron injection from the cathode into the fullerene LUMO. The results of the experiments are presented in Table 2, followed by the SCLC curve fits in Figure 10.

As can be seen, there are considerable differences in the hole mobility depending on the processing conditions, with DCB based devices exhibiting higher mobilities than CB based devices. Most interesting is the disparity in hole mobility for the heat treated, CB based devices, with the P3HT:bis-ThCBM device displaying a lower mobility. It would appear that the second addend and poly-isomerism of the bis-ThCBM acts to inhibit the crystallising tendencies of the P3HT to a greater extent than PCBM. This correlates with J-V results of devices spin cast from CB where devices containing bis-ThCBM typically exhibit slightly lower fill factors. However, this hole-mobility deficit is recovered when DCB is used as the spin casting solvent, indicating that the slow drying technique allows the bis-THCBM and P3HT time to orient in a more ordered way before the solvent evaporates and locks the morphology in place.

The results show there is no significant difference between the hole mobilities of the bis-ThCBM and PCBM based devices spin cast from DCB, suggesting that improved hole mobility is not responsible for the improved fill factor and reduced series current in bis-ThCBM based devices.

Fullerene Derivative	Solvent	Heat Treatment	Hole Mobility, x 10^{-7} m^2/V.s
Bis-ThCBM	CB	Yes	0.11 ± 0.02
	DCB	No	0.74 ± 0.05
PCBM	CB	Yes	0.19 ± 0.04
	DCB	no	0.70 ± 0.02

Table 2. Hole Mobility Results for bis-ThCBM and PCBM based P3HT devices. Heat treated samples were annealed on a hotplate under nitrogen at 150°C for 5 minutes

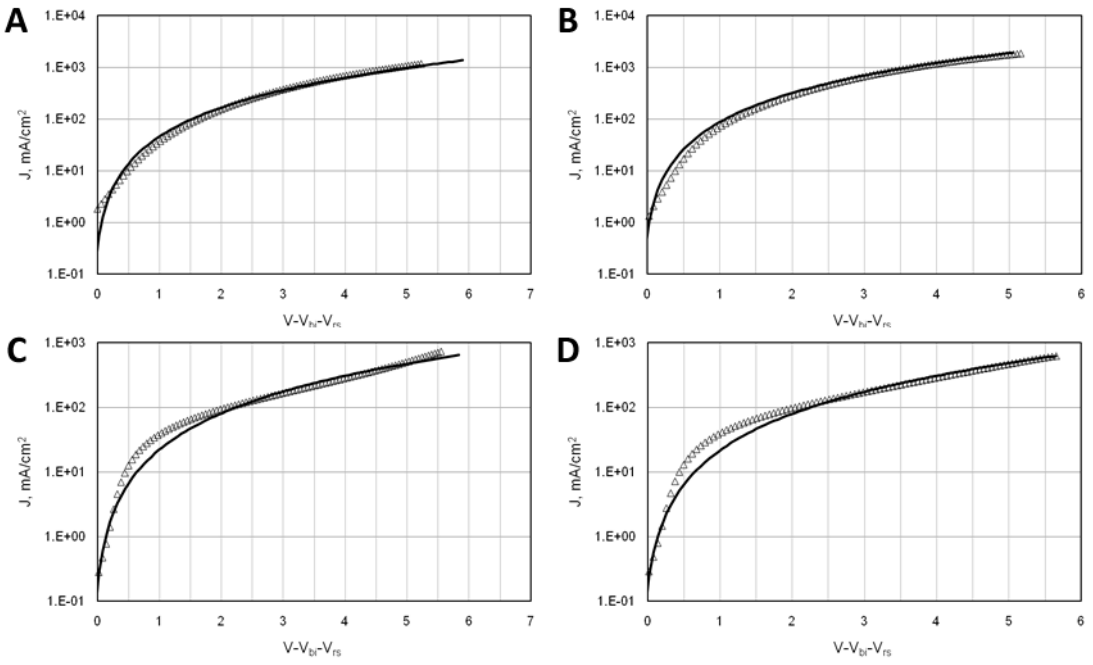

Figure 10. SCLC Curve fits for hole only P3HT:bis-ThCBM and P3HT:PCBM devices. A) P3HT:bis-ThCBM spin cast from CB heat treated at 150°C. B) P3HT:PCBM spin cast from CB heat treated at 150°C for 10 minutes. C) P3HT:bis-ThCBM spin cast from DCB, no HT. D) P3HT:PCBM spin cast from DCB, no HT.

VII.V Critical Field Measurements on P3HT:fullerene solar cells

To further probe the effect of bis-THCBM on P3HT based solar cells, critical field measurements were carried out, as outlined in Chapter 3. The idea of the critical field, F_C, was introduced by Marsh et al where the authors sought a simple model to explain the I-V curves of a range of excitonic solar cells, including P3HT:PCBM.[35] Using the superposition approximation, it is possible to curve fit the model to the photocurrent from an I-V curve taken under monochromatic light. The single fitted parameter, F_C, denotes the electrical field required to separate 50% of the germinate charge pairs dissociated across the polymer/fullerene heterojunction. In the current work, this model was used to determine the critical field values for representative P3HT:PCBM and P3HT:bis-THCBM devices spin cast from DCB, over a range of wavelengths, making this the first exploration of F_C as a function of wavelength. The results are presented in Figure 11.

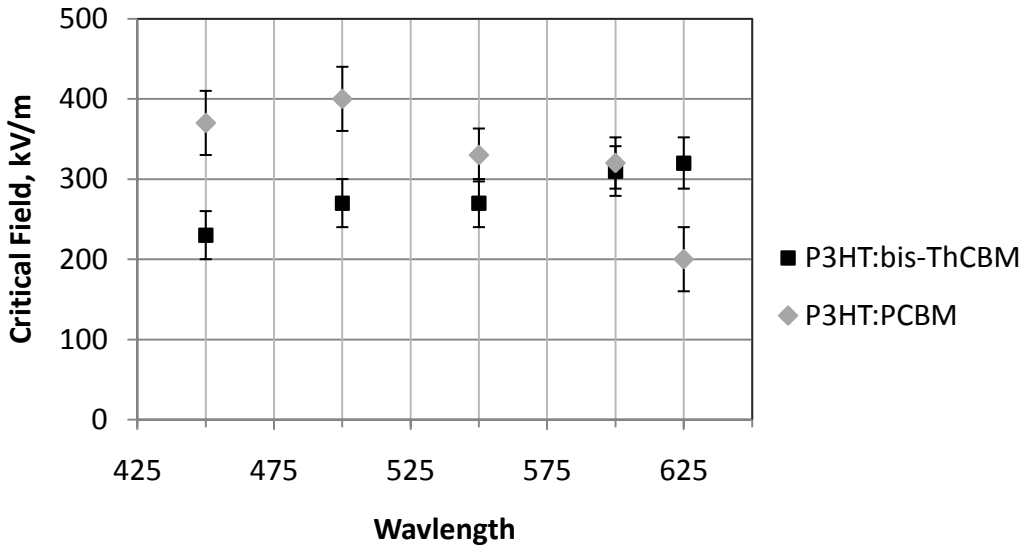

Figure 11. Calculated Critical Field Values for P3HT:bis-THCBM and P3HT:PCBM based devices, spin cast from DCB with LiF/Al cathode. P3HT:fullerene ratio of 1:1.3. The raw data and fits used for Figure 10 are presented in Appendix VI.IX.IV

Firstly, the results show that F_C varies as a function of wavelength. Although the illuminating beam intensity also varies as a function of wavelength, this can be ruled out influencing the F_C values as Marsh et al showed that F_C is independent of intensity over three orders of magnitude, whereas the incident intensities here vary by less than one order of magnitude.

One possible explanation relates to the heat generated by the process of thermalisation. Photons with energy greater than the polymer band gap excite electrons above the polymer LUMO and thermalisation refers to the phonon-assisted relaxation of these 'hot' electrons to the polymer band edge via thermal emission. Using Braun's theoretical description of charge separation,[36] Marsh et al. proposed that the F_C can be described by the equation

$$F_C \propto \frac{r_0^3 v_r}{\langle\mu\rangle r_c^2} \exp\left(\frac{r_C}{r_0}\right) \quad (2)$$

Where r_0 is the exciton bond length, v_r the rate constant of recombination of germinate pairs across the heterojunction, $\langle\mu\rangle$ the spatially averaged sum of electron and hole mobility in the device, and r_C the thermal capture radius equivalent to:

$$r_C = \frac{e^2}{4\pi\langle\varepsilon\rangle\varepsilon_0 kT} \quad (3)$$

Where ,$\langle\varepsilon\rangle$ is the spatially averaged dielectric constant of the polymer and fullerene species. The temperature dependence of F_C is therefore highly dependent on the ratio of r_C/r_0. At room temperature r_C is on the order of 1.1×10^{-8}m ($\langle\varepsilon\rangle$= 5.2, taken

as the mean of the fullerene (3.9) and P3HT (6.5)[37] dielectric constants) whereas, r_0, the exciton bond length is considerably smaller. As a result, F_C exhibits a large negative dependence on temperature, suggesting that thermalisation of 'hot' electrons, which varies as a function of wavelength, could affect its value.

The second observation that can be made is that the bis-THCBM based device has significantly lower F_C values at smaller wavelengths. This matches with the observation of a greater relative EQE for bis-THCBM based devices at lower wavelengths as shown in Figure 11, and the improved fill factor at greater layer thickness. A reduced critical field means increased charge separation efficiency and reduced germinate recombination of charge carriers across the polymer/fullerene interface. This in turn leads to improved charge extraction, for a given charge transport environment. As noted by Marsh et al, optimised polymer:fullerene solar cells, such as those presented here, exhibit a linear dependence of the J_{SC} on the intensity of the exciting radiation which indicates that germinate recombination is the dominant loss mechanism.[35] The fact that these results show a correlation between F_C and EQE at low wavelengths (Figure 12) is further evidence of this. If germinate recombination was not the limiting factor in these devices, an improvement in F_C would not manifest as an improvement in EQE.

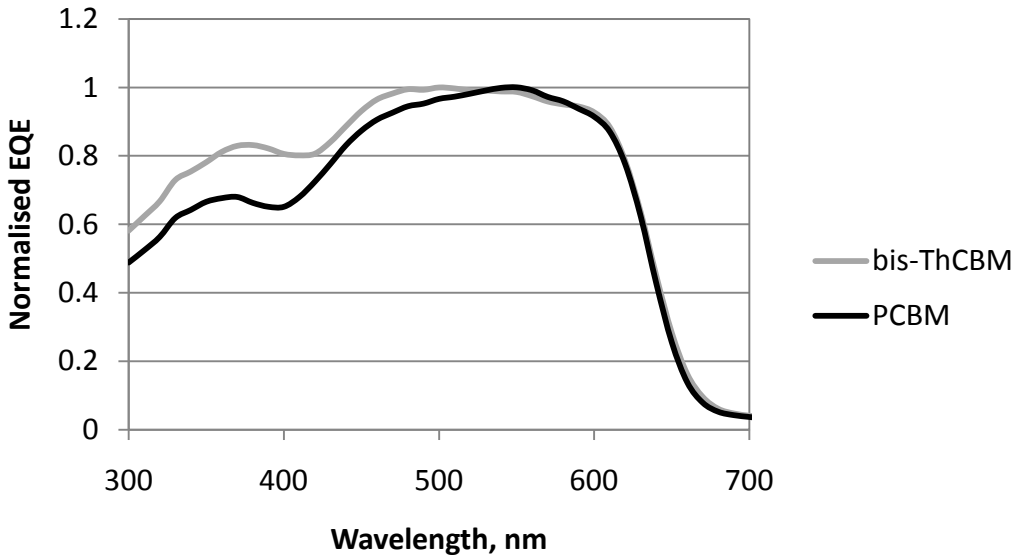

Figure 12. Normalised EQE spectra of P3HT:bis-ThCBM and P3HT:PCBM based devices spin cast from DCB, with a LiF/Al cathode. The P3HT:fullerene weight ratio is 1:1.3 for both devices.

VII.VI Temperature Dependent EQE Experiments on P3T:bis-ThCBM solar cells

Further understanding of the heightened EQE at low wavelengths in bis-ThCBM based devices was sought through the use of temperature dependent EQE experiments. By plotting the log of the short circuit current for a given wavelength as a function of inverse temperature, an activation energy can be extracted which relates to the temperature dependent processes within the device.[38] These processes include exciton diffusion, exciton dissociation, separation of the bound germinate pair, charge transport and charge transfer at the electrodes. The extracted activation energy reflects an agglomeration of the independent activation energies of each of these processes.[38] The last three processes are similar regardless of whether an exciton is generated in the polymer or fullerene phase. However, the

first two may differ significantly and by investigating two different wavelengths characteristic of PCBM and P3HT absorption, exciton mobility and dissociation in both the PCBM (350nm) and P3HT (500nm) can be investigated independently. Comparisons can also be made between separate devices, but are complicated by the fact that all five of the thermally dependent processes must be taken into account.

The results of the experiment are shown in Figure 13 and it can be seen that at 500nm, the activation energy in the bis-THCBM based devices appears to be higher (2.4 ± 0.3 meV) than for the PCBM based devices (1.3 ± 0.3 meV) . This is most likely caused by the slightly reduced electron mobility in the bis-ThCBM phase, compared to PCBM, as discussed in section VI.II.I. It is also possible that the reduced $LUMO_{donor}$ - $LUMO_{acceptor}$ offset in the P3HT:bis-ThCBM system, as a result of bis-ThCBM's raised LUMO, may be playing a role by reducing the driving force for exciton dissociation.

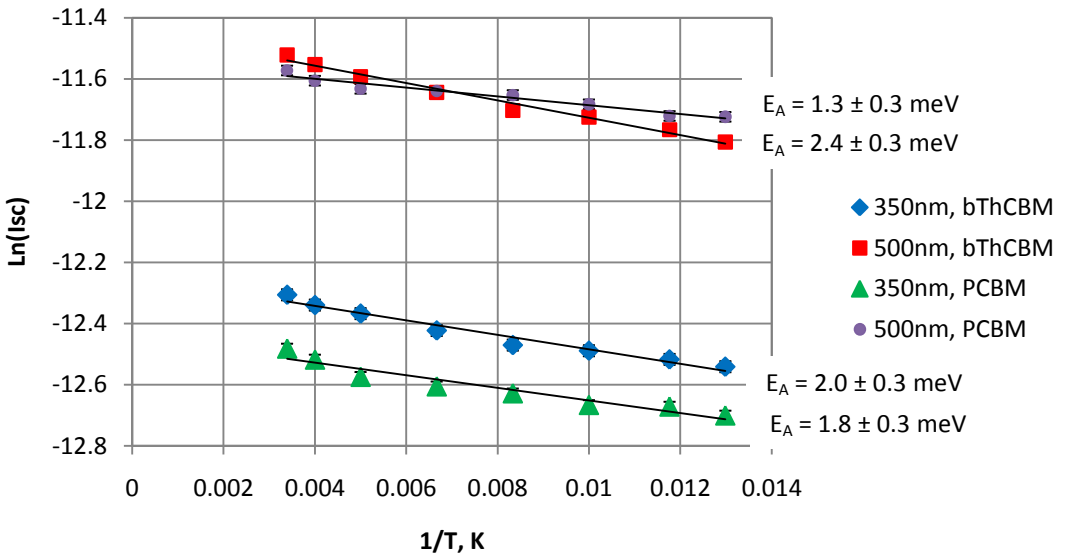

Figure 13. Calculated E_a values of bis-ThCBM and PCBM based devices obtained from excitation at 350nm and 500nm. Spin cast from DCB, with LiF/Al electrode.

Regardless, of the exact cause, it is clear that the introduction of bis-ThCBM has some negative effects on the device physics aside from the benefits of an enhanced V_{OC} and improved germinate separation.

Surprisingly, at 350nm, there is no significant difference in the agglomerated activation energies for devices incorporating the two different fullerene species. One might expect to see a higher activation energy for the bis-ThCBM based device, as observed at 500nm, since the free electron that results from an exciton generated in the fullerene phase must still drift through the same lower mobility pathways as a free electron generated from the polymer.

This result suggests that the effect of the reduced electron mobility is being cancelled out by an improvement in another, fullerene specific process; fullerene exciton diffusion or dissociation. Considering the increased disorder in the bis-

ThCBM phase (indicated by its lower electron mobility), it is unlikely that exciton diffusion is in any way improved beyond that found in PCBM. This suggests that the incorporation of bis-ThCBM leads to a reduction in the activation energy associated with fullerene exciton dissociation, possibly due to improved pi-orbital overlap between the polymer and the fullerene thienyl moiety.

Although a great amount of work has been published investigating the ultra fast electron transfer from conjugated polymers to fullerenes[39,40] hole transfer from fullerenes to polymers has garnered less interest due to its historically minor contribution to the overall photocurrent. This bias will need to be as addressed as fullerenes with improved absorption properties, such as $PC_{71}BM$ are increasingly used in polymer:fullerene solar cells.

VII.VII Conclusions

In conclusion, this chapter covers an extensive comparison of the use of bis-ThCBM and PCBM in P3HT based photovoltaics. The results show that given the correct choice of spin casting solvent and cathode composition, bis-ThCBM can be used to produce photovoltaic devices with efficiencies in excess of those achievable with PCBM (4.6% vs. 3.6%). The primary reason for this is the notable higher V_{OC} obtained with bis-ThCBM due to its raised LUMO. The remainder of the improvement can be attributed to the reduced critical field observed in the bis-THCBM devices, and possibly an improvement in the charge separation of fullerene generated excitons.

These effects manifests as an improved EQE at lower wavelengths and a slightly higher fill factor.

The overall improvement in device efficiency is obtained despite a slight reduction in electron mobility in the bis-ThCBM, which most likely causes an increase in the agglomerated activation energy for polymer generated extracted charge carriers.

It is worth noting that the efficiency benefits observed in devices incorporating bis-ThCBM are only achieved with the use of a high boiling point solvent, in this case DCB, and a non-continuous LiF layer at the polymer/cathode interface.

VII.VIII References

[1] Scharber, M. C. *et al.* Design Rules for Donors in Bulk-Heterojunction Solar Cells - Towards 10 % Energy-Conversion Efficiency. *Advanced Materials* **18**, 789-794 (2006).

[2] Rand, B. P., Burk, D. P. & Forrest, S. R. Offset energies at organic semiconductor heterojunctions and their influence on the open-circuit voltage of thin-film solar cells. *Physical Review B (Condensed Matter and Materials Physics)* **75**, 115327 (2007).

[3] Brabec, C. J. *et al.* Origin of the Open Circuit Voltage of Plastic Solar Cells. *Advanced Functional Materials* **11**, 374-380 (2001).

[4] Lacramioara, M. P., Patrick van 't, H., Alexander, B. S., Harry, T. J. & Jan, C. H. Thienyl analog of 1-(3-methoxycarbonyl)propyl-1-phenyl-[6,6]-methanofullerene for bulk heterojunction photovoltaic devices in combination with polythiophenes. *Applied Physics Letters* **89**, 213507 (2006).

[5] Porfyrakis, K. (2009).

[6] Chang, J.-F. *et al.* Enhanced Mobility of Poly(3-hexylthiophene) Transistors by Spin-Coating from High-Boiling-Point Solvents. *Chemistry of Materials* **16**, 4772-4776, doi:doi:10.1021/cm049617w (2004).

[7] Li, G. *et al.* High-efficiency solution processable polymer photovoltaic cells by self-organization of polymer blends. *Nat Mater* **4**, 864-868 (2005).

[8] Martijn Lenes, G.-J. A. H. W. F. B. K. S. C. V. J. C. H. P. W. M. B. Fullerene Bisadducts for Enhanced Open-Circuit Voltages and Efficiencies in Polymer Solar Cells. *Advanced Materials* **20**, 2116-2119 (2008).

[9] V.D. Mihailetchi, J. K. J. v. D. P. W. M. B. J. C. H. R. A. J. J. J. M. K. M. T. Electron Transport in a Methanofullerene. *Advanced Functional Materials* **13**, 43-46 (2003).

[10] Mihailetchi, V. D. *et al.* Electron Transport in a Methanofullerene. *Advanced Functional Materials* **13**, 43-46 (2003).

[11] Popescu, L. M., Hof, P. v. t., Sieval, A. B., Jonkman, H. T. & Hummelen, J. C. Thienyl analog of 1-(3-methoxycarbonyl)propyl-1-phenyl-[6,6]-methanofullerene for bulk heterojunction photovoltaic devices in combination with polythiophenes. *Applied Physics Letters* **89**, 213507 (2006).

[12] Ma, W., Yang, C., Gong, X., Lee, K. & Heeger, A. J. Thermally Stable, Efficient Polymer Solar Cells with Nanoscale Control of the Interpenetrating Network Morphology. *Advanced Functional Materials* **15**, 1617-1622 (2005).

[13] Campoy-Quiles, M. *et al.* Morphology evolution via self-organization and lateral and vertical diffusion in polymer:fullerene solar cell blends. *Nat Mater* **7**, 158-164 (2008).

[14] Rispens, M. T. *et al.* Influence of the solvent on the crystal structure of PCBM and the efficiency of MDMO-PPV:PCBM 'plastic' solar cells. *Chemical Communications*, 2116-2118 (2003).

[15] Ouml, sterbacka, R., An, C. P., Jiang, X. M. & Vardeny, Z. V. Two-Dimensional Electronic Excitations in Self-Assembled Conjugated Polymer Nanocrystals. *Science* **287**, 839-842, doi:10.1126/science.287.5454.839 (2000).

[16] Zhokhavets, U., Erb, T., Gobsch, G., Al-Ibrahim, M. & Ambacher, O. Relation between absorption and crystallinity of poly(3-hexylthiophene)/fullerene films for plastic solar cells. *Chemical Physics Letters* **418**, 347-350 (2006).

[17] Mihailetchi, V. D., Blom, P. W. M., Hummelen, J. C. & Rispens, M. T. Cathode dependence of the open-circuit voltage of polymer:fullerene bulk heterojunction solar cells. *Journal of Applied Physics* **94**, 6849-6854 (2003).

[18] Hoppe, H. & Sariciftci, N. S. OrganicSolar Cells: An Overview. *Journal of Materials Research* **19** (2004).

[19] Hide, J. G. F. & Wang, H. Efficient photodetectors and photovoltaic cells from composites of fullerenes and conjugated polymers: photoinduced electron transfer. *Synthetic Metals* **84**, 979-980 (1997).

[20] Liu, J., Shi, Y. & Yang, Y. Solvation-Induced Morphology Effects on the Performance of Polymer-Based Photovoltaic Devices. *Advanced Functional Materials* **11**, 420-424 (2001).

[21] Hoppe, H. *et al.* Nanoscale Morphology of Conjugated Polymer/Fullerene-Based Bulk- Heterojunction Solar Cells. *Advanced Functional Materials* **14**, 1005-1011 (2004).

[22] Xu, Z. *et al.* Vertical Phase Separation in Poly(3-hexylthiophene): Fullerene Derivative Blends and its Advantage for Inverted Structure Solar Cells. *Advanced Functional Materials* **19**, 1227-1234 (2009).

[23] Li, G. *et al.* Solvent Annealing Effect in Polymer Solar Cells Based on Poly(3-hexylthiophene) and Methanofullerenes. *Advanced Functional Materials* **17**, 1636-1644 (2007).

[24] Li, G., Shrotriya, V., Yao, Y. & Yang, Y. Investigation of annealing effects and film thickness dependence of polymer solar cells based on poly(3-hexylthiophene). *Journal of Applied Physics* **98**, 043704 (2005).

[25] Inoue, K. *et al.* Temperature and Time Dependence of Heat Treatment of RR-P3HT/PCBM Solar Cell. *Synthetic Metals* **154**, 41-44 (2005).

[26] Kim, H., So, W.-W. & Moon, S.-J. The importance of post-annealing process in the device performance of poly(3-hexylthiophene): Methanofullerene polymer solar cell. *Solar Energy Materials and Solar Cells* **91**, 581-587 (2007).

[27] Kim, H. J., Lee, H. H. & Kim, J.-J. Real Time Investigation of the Interface between a P3HT:PCBM Layer and an Al Electrode during Thermal Annealing. *Macromolecular Rapid Communications* **30**, 1269-1273 (2009).

[28] Hung, L. S., Tang, C. W. & Mason, M. G. Enhanced electron injection in organic electroluminescence devices using an Al/LiF electrode. *Applied Physics Letters* **70**, 152-154 (1997).

[29] Jabbour, G. E. *et al.* Highly efficient and bright organic electroluminescent devices with an aluminum cathode. *Applied Physics Letters* **71**, 1762-1764 (1997).

[30] Shaheen, S. E. *et al.* Bright blue organic light-emitting diode with improved color purity using a LiF/Al cathode. *Journal of Applied Physics* **84**, 2324-2327 (1998).

[31] Yoon, J., Kim, J.-J., Lee, T.-W. & Park, O.-O. Evidence of band bending observed by electroabsorption studies in polymer light emitting device with ionomer/Al or LiF/Al cathode. *Applied Physics Letters* **76**, 2152-2154 (2000).

[32] Brown, T. M. *et al.* LiF/Al cathodes and the effect of LiF thickness on the device characteristics and built-in potential of polymer light-emitting diodes. *Applied Physics Letters* **77**, 3096-3098 (2000).

[33] Brabec, C. J., Shaheen, S. E., Winder, C., Sariciftci, N. S. & Denk, P. Effect of LiF/metal electrodes on the performance of plastic solar cells. *Applied Physics Letters* **80**, 1288-1290 (2002).

[34] Jonsson, S. K. M., Carlegrim, E., Zhang, F., Salaneck, W. R. & Fahlman, M. Photoelectron spectroscopy of the contact between the cathode and the active layers in plastic solar cells: The role of LiF. *Jpn. J. Appl. Phys. Part 1 - Regul. Pap. Short Notes Rev. Pap.* **44**, 3695-3701, doi:10.1143/jjap.44.3695 (2005).

[35] Marsh, R. A., McNeill, C. R., Abrusci, A., Campbell, A. R. & Friend, R. H. A Unified Description of Currentâ€“Voltage Characteristics in Organic and Hybrid Photovoltaics under Low Light Intensity. *Nano Letters* **8**, 1393-1398, doi:10.1021/nl080200p (2008).

[36] Braun, C. L. Electric field assisted dissociation of charge transfer states as a mechanism of photocarrier production. *The Journal of Chemical Physics* **80**, 4157-4161 (1984).

[37] Estrada, M., Mejia, I., Cerdeira, A. & Iñiguez, B. MIS polymeric structures and OTFTs using PMMA on P3HT layers. *Solid-State Electronics* **52**, 53-59 (2008).

[38] Kim, K., Liu, J., Namboothirym, M. A. G. & Carroll, D. Roles of donor and acceptor nanodomains in 6% efficient thermally annealed polymer photovoltaics. *Applied Physics Letters* **90** (2007).

[39] Kraabel, B. *et al.* Ultrafast photoinduced electron transfer in conducting polymer--buckminsterfullerene composites. *Chemical Physics Letters* **213**, 389-394 (1993).

[40] Sariciftci, N. S., Smilowitz, L., Heeger, A. J. & Wudl, F. Photoinduced Electron Transfer from a Conducting Polymer to Buckminsterfullerene. *Science* **258**, 1474-1476, doi:10.1126/science.258.5087.1474 (1992).

VII.IX Appendix

Appendix VI.IX.I Comparisons of Measured and EQE Estimated Jsc for P3HT:bis ThCBM, DCB, LiF

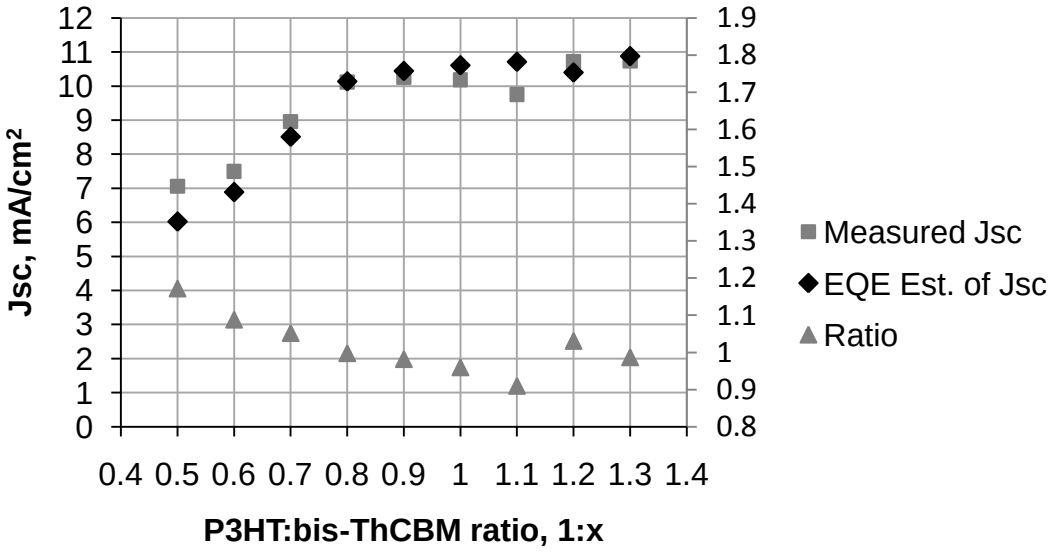

Appendix VI.IX.II Comparisons of Measured and EQE Estimated Jsc for P3HT:PCBM, DCB, LiF

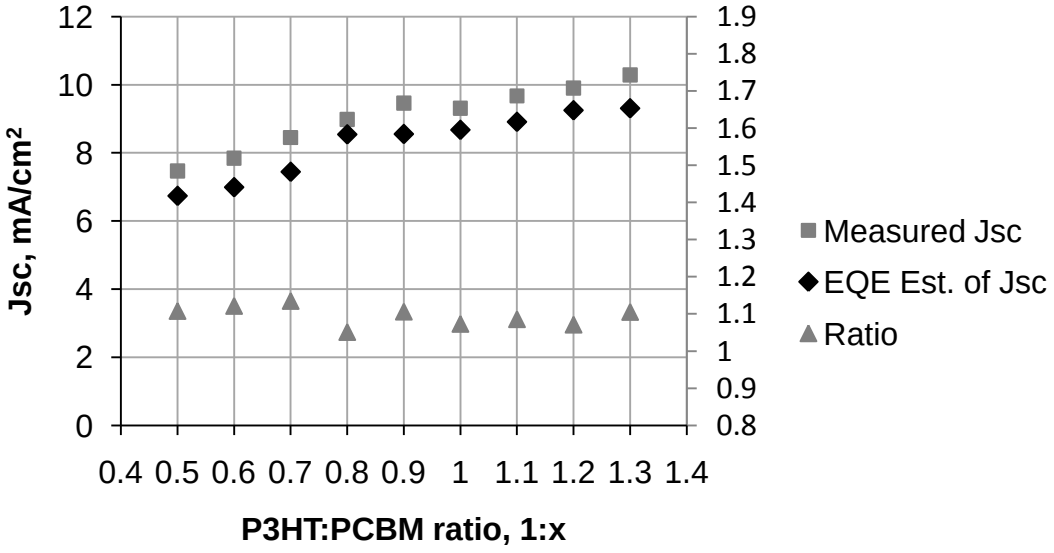

Appendix VI.IX.III Temperature Dependent EQE curves of P3HT:bis-ThCBM (top) and P3HT:PCBM (bottom) devices. Spin cast from DCB. P3HT:fullerene weight ratio of 1:1.3

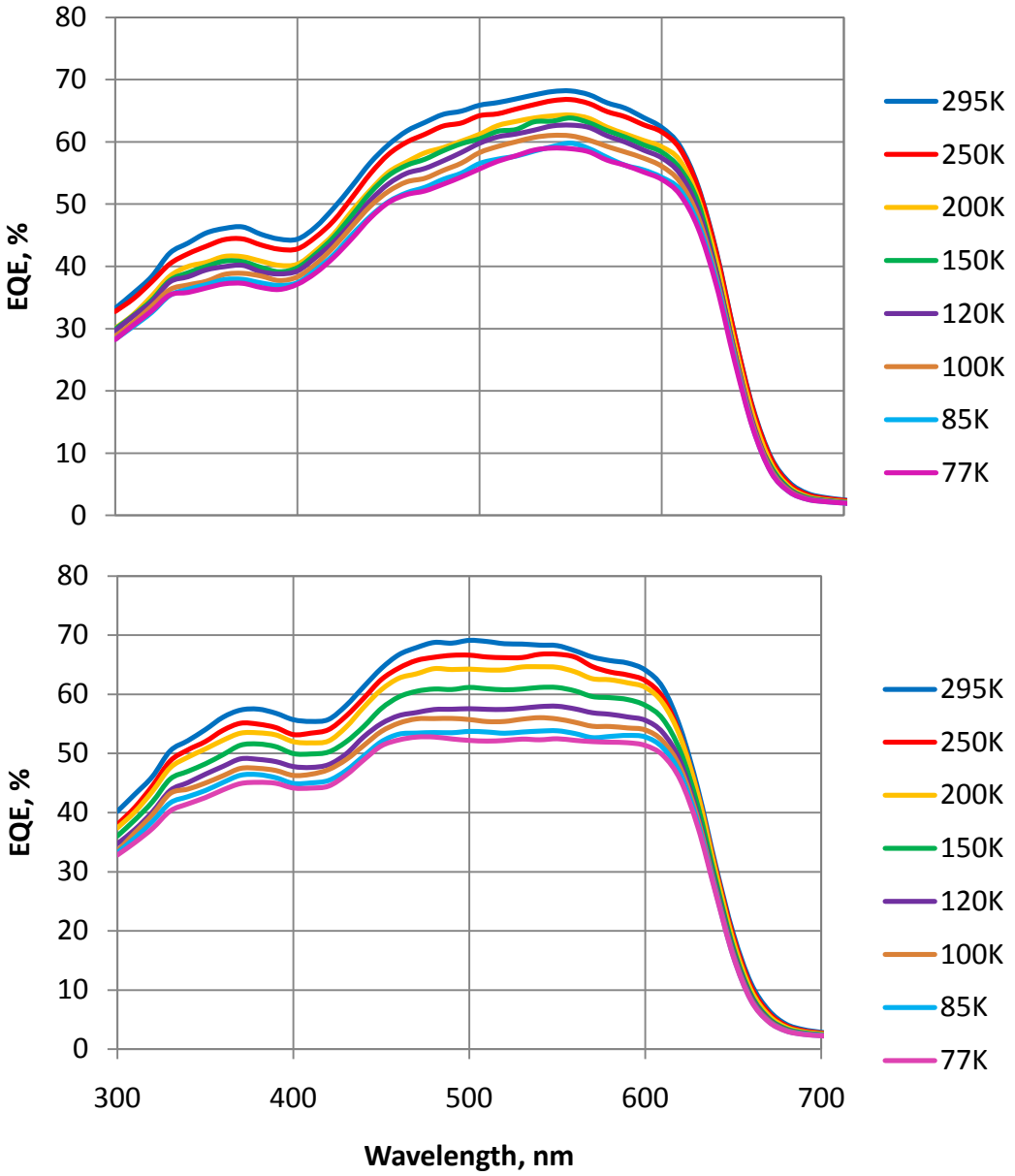

Appendix VI.IX.IV Fitted Curves for the Critical Field Measurements presented in Figure 10.

VI.IX.IV.I P3HT:bis-ThCBM based Devices

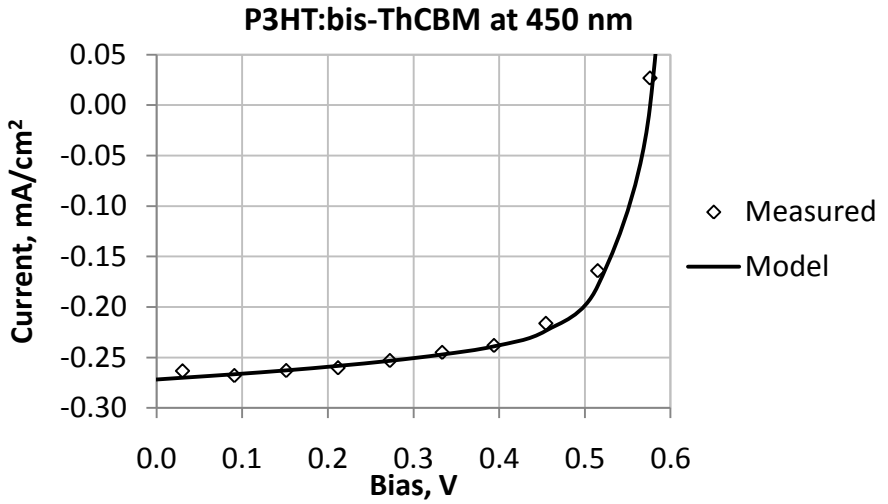

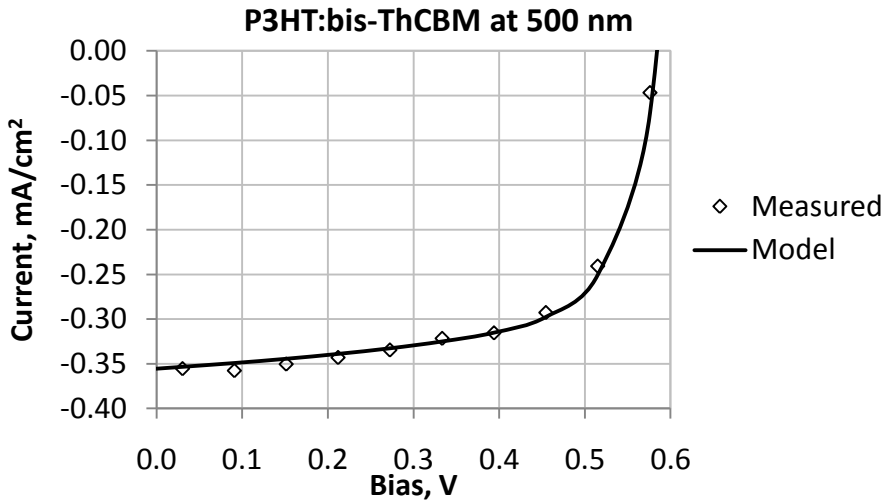

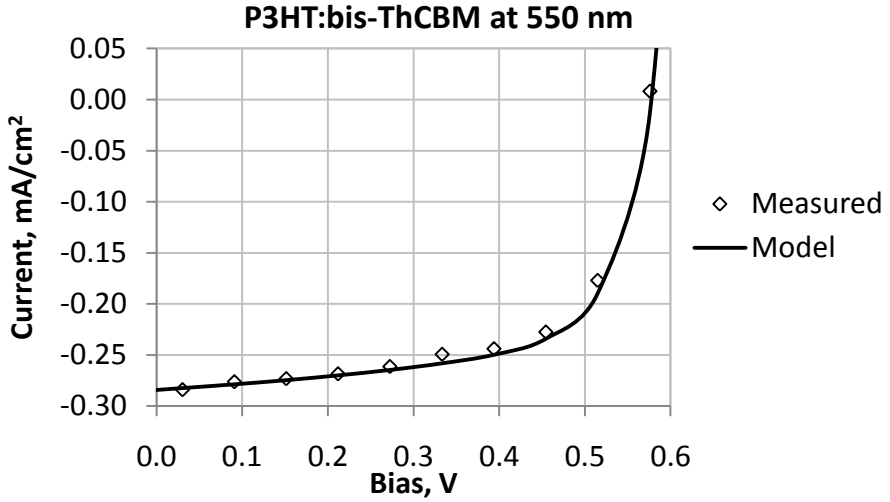
P3HT:bis-ThCBM at 550 nm
Current, mA/cm²
0.05
0.00
-0.05
-0.10
-0.15
-0.20
-0.25
-0.30
0.0
0.1
0.2
0.3
0.4
0.5
0.6
Bias, V
Measured
Model

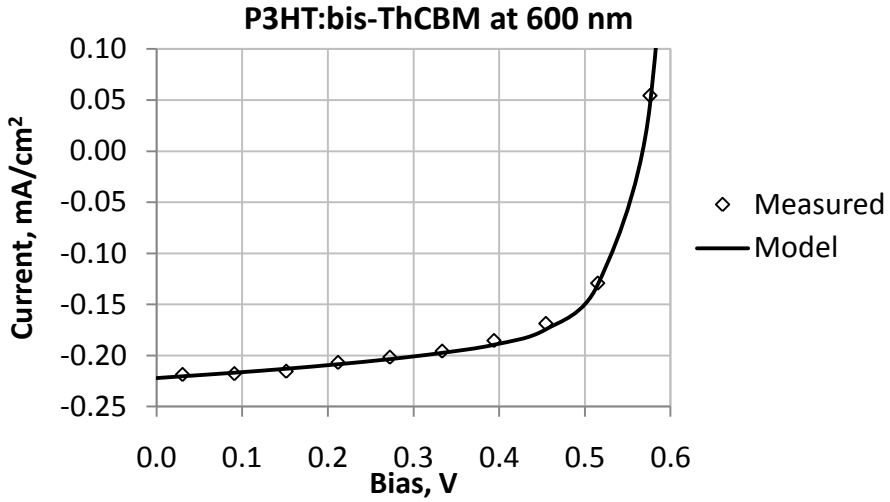
P3HT:bis-ThCBM at 600 nm
Current, mA/cm²
0.10
0.05
0.00
-0.05
-0.10
-0.15
-0.20
-0.25
0.0
0.1
0.2
0.3
0.4
0.5
0.6
Bias, V
Measured
Model

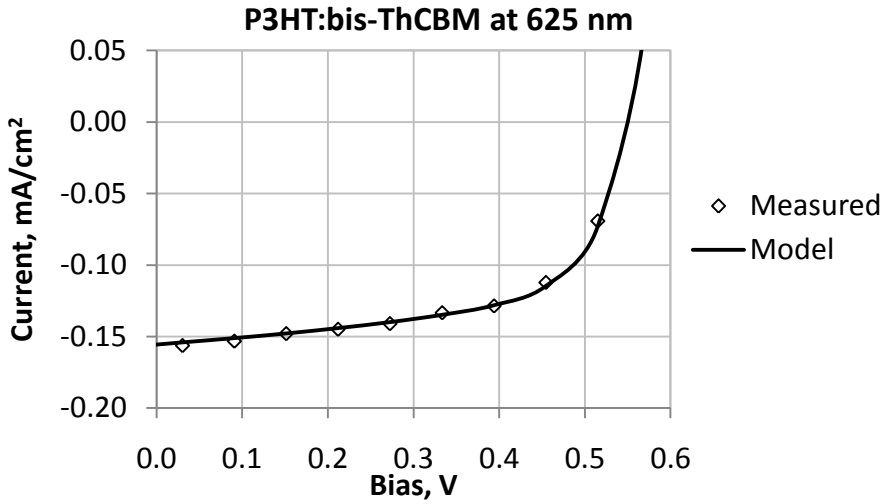
P3HT:bis-ThCBM at 625 nm
Current, mA/cm²
0.05
0.00
-0.05
-0.10
-0.15
-0.20
0.0
0.1
0.2
0.3
0.4
0.5
0.6
Bias, V
Measured
Model

VI.IX.IV.II P3HT:PCBM based Devices

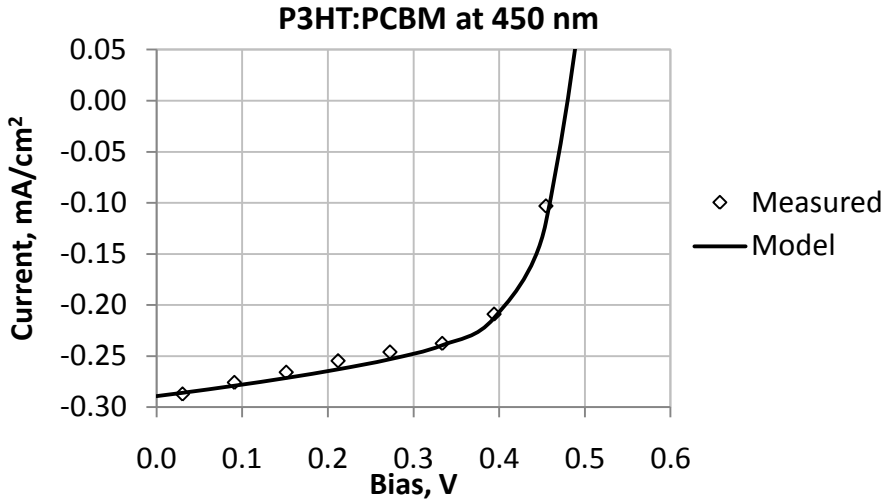

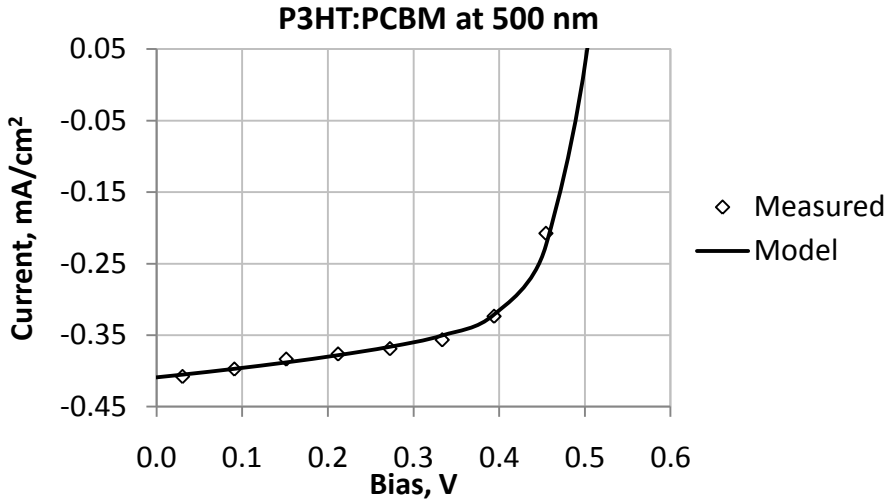

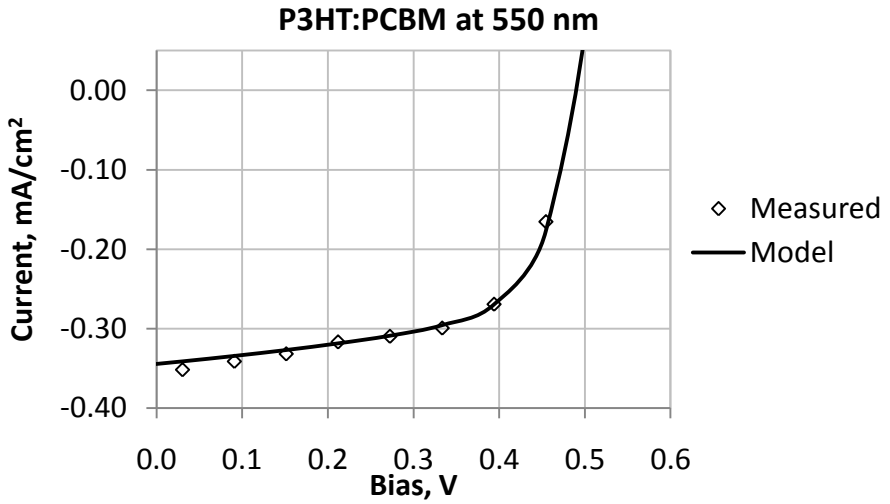

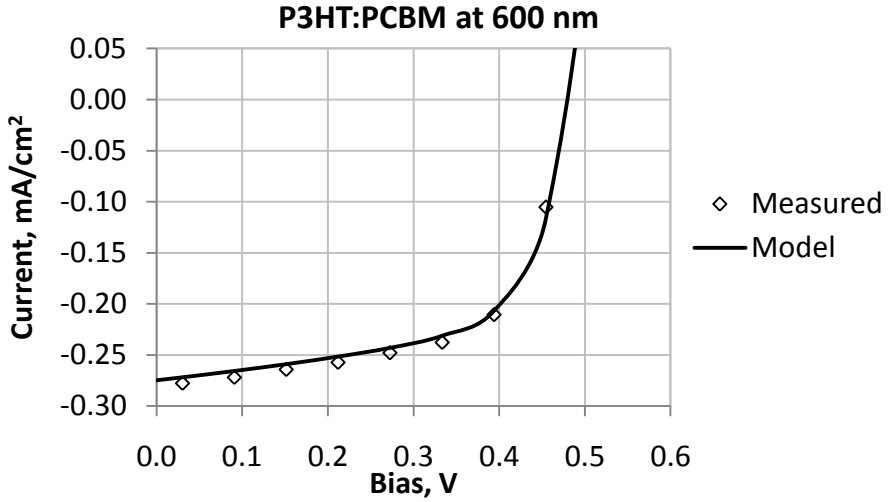
P3HT:PCBM at 600 nm
Current, mA/cm²
0.05
0.00
-0.05
-0.10
-0.15
-0.20
-0.25
-0.30
0.0
0.1
0.2
0.3
0.4
0.5
0.6
Bias, V
Measured
Model

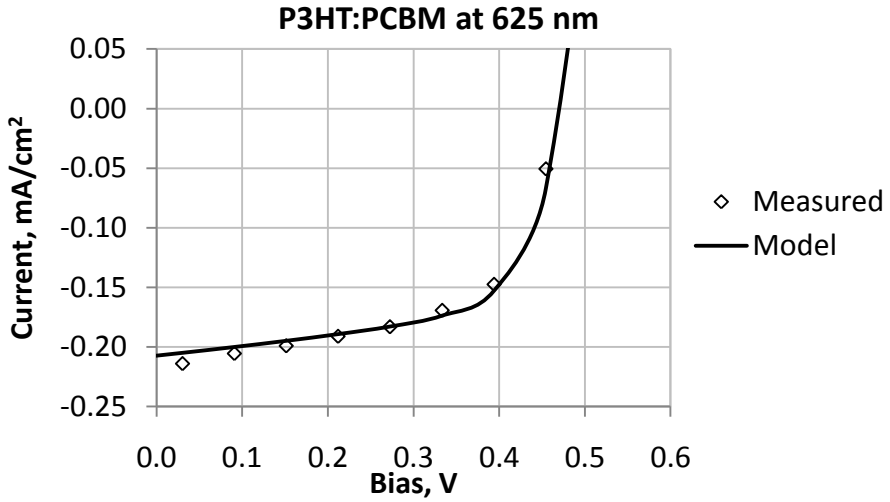
P3HT:PCBM at 625 nm
Current, mA/cm²
0.05
0.00
-0.05
-0.10
-0.15
-0.20
-0.25
0.0
0.1
0.2
0.3
0.4
0.5
0.6
Bias, V
Measured
Model